BIOCOMPATIBILITY AND TOXICITY STUDIES ON HETEROGENEOUS TiO_2-ZNO POLYMER NANOCOMPOSITE WITH ENHANCED BACTERIAL ACTIVITY

NOR HAZLIANA BINTI HARUN

UNIVERSITI SAINS MALAYSIA

2022

BIOCOMPATIBILITY AND TOXICITY STUDIES ON HETEROGENEOUS TIO_2-ZNO POLYMER NANOCOMPOSITE WITH ENHANCED BACTERIAL ACTIVITY

by

NOR HAZLIANA BINTI HARUN

Thesis submitted in fulfilment of the requirements
for the degree of
Doctor of Philosophy

July 2022

ACKNOWLEDGEMENT

In the name of Allah S.W.T., the Most Gracious, the Most Merciful. All praises and gratitude belongs to Allah, the sources of my strength in completing the thesis throughout this semester despite Covid-19 challenges. First and foremost, I wish to express my sincerest gratitude to my dedicated supervisor, Ts. Dr. Rabiatul Basria S.M.N. Mydin, for her continuous support, her patience and she consistently guide me in the right direction whenever she thought I needed it. I would also like to express my gratitude to my great co-supervisors, Prof Ir Dr Srimala Sreekantan and Prof. Madya Md Azman Seeni Mohamed for helping me especially in providing financial assistance and ideas despite their busy schedules. May Allah S.W.T. grants the best rewards for these great people. Besides, I would also like to take this opportunity to express my thanks to those people who have helped me throughout my research period, especially from Animal Research Complex (ARC) and Clinical Trial Complex (CTC), USM AMDI in providing services and facilities for this research to be well conducted. I will not also forget the help obtained from Dr. Siti Salmah Noordin, which without her, I may not be able to even perform blood collection for haemocompatibility testing. I would also like to extend my gratitude to intern students, juniors and seniors which involved in my research. Lastly, I would like to express my deepest gratitude to my beloved parents, family members, friends and colleagues for their unfailing support, prayers and encouragement through the process of researching and writing this thesis. Allhamdulillah ‘ala kulli hal.

TABLE OF CONTENTS

ACKNOWLEDGEMENT…..... ii

TABLE OF CONTENTS…..... iii

LIST OF TABLES..... viii

LIST OF FIGURES..... x

LIST OF UNITS AND SYMBOLS..... xx

LIST OF ABBREVIATIONS..... xxi

LIST OF APPENDICES..... xxv

ABSTRAK..... xxvi

ABSTRACT..... xxviii

CHAPTER 1 INTRODUCTION..... 1

1.1 Research background..... 1

1.2 Research objectives..... 3

1.2.1 General objective..... 3

1.2.2 Specific objectives..... 3

CHAPTER 2 LITERATURE REVIEW..... 5

2.1 Biomedical devices and healthcare associated infections……... 5

2.1.1 Multidrug resistant and non-multidrug resistant HAIs pathogen issues…….. 9

2.1.2 Biofilm development issues related to medical devices…….... 11

2.2 Present status of synthetic biomedical polymers…… 16

2.2.1 Implementation of metal oxide nanoparticles in biomedical polymers…… 19

2.2.2 Antibacterial potential of TiO_2 and ZnO nanocomposites…... 23

2.3 Testing guidelines for polymer based nanocomposite…… 26

2.3.1 Antibacterial profiles……. 26

2.3.2 Biocompatibility profiles…….. 29

2.3.3 Haemocompatibility profiles……. 33

CHAPTER 3 METHODOLOGY…….. 36

3.1 Introduction……. 36

3.2 Materials and chemicals…….. 36

3.3 Synthesis and preparation of materials……... 37

3.3.1 Experimental workflow……. 38

3.4 Antibacterial profiles…….. 39

3.4.1 Bacterial strains and culture media……... 39

3.4.2 Kirby-Bauer disk diffusion assay…….. 39

3.4.3 Minimum inhibitory concentration (MIC) and minimum bactericidal concentration (MBC) …… 40

3.4.4 Time-kill activity……... 41

3.4.5 Assessment of biofilm formation…….. 41

3.4.6 ASTM E2149…… 42

3.5 *In vitro* cytotoxicity assay according to ISO 10993: Part 5…… 42

3.5.1 Maintenance of cells in culture and cell counting……. 43

3.5.2. Cell viability assay…… 44

3.5.3 Cell membrane integrity…… 45

3.5.4 Colony formation assay……. 46

3.6 Biochemical profiles……... 47

3.6.1 Intracellular reactive oxygen species production…….. 47

3.6.2 Hoechst and Calcein-AM staining…… 48

3.6.3 Metal ion release study……. 48

3.7 Gene expression profiles by Real-Time PCR……. 50

3.7.1 RNA extraction, quantification and quality check…… 50

3.7.2 Reverse transcription reaction……... 51

3.7.3 SYBR green-based Real-Time PCR system……. 52

3.8 Protein analysis…….. 54

3.8.1 Protein extraction and quantification…… 54

3.8.2 Protein separation and transferring from gel to PVDF membrane…….. 54

3.8.3 Immuno-blotting against the targeted protein……... 55

3.8.4 Chemiluminescent imaging and data analysis…….. 55

3.9 In vitro haemocompatibility testing according to ISO 10993: Part 4……. 56

3.9.1 Blood collection and preparation of whole blood, red blood cells suspension and platelet poor plasma……. 56

3.9.2 Full blood counts and coagulation assay……... 56

3.9.3 Whole blood clotting kinetics……... 57

3.9.4 *In vitro* haemolysis assessment……. 57

3.9.5 Platelet adhesion study…….. 58

3.10 Field Emission Scanning Electron Microscopy…….. 59

3.10.1 Bacterial cell adhesion…….. 59

3.10.2 Cell adhesion and attachment…… 59

3.10.3 Whole blood and fibrin attachment……... 60

3.11 Functional time frame of LLDPE nanocomposite films…… 60

3.11.1 *In vitro* degradation assay……. 60

3.11.2 Hydrolytic degradation assay…… 61

3.11.3 Soil burial assay…… 62

CHAPTER 4 RESULTS……. 64

4.1 Introduction……. 64

4.2 Description for study materials……... 64

4.3 Measurement of antibacterial profiles…… 65

4.3.1 Kirby-Bauer disk diffusion assay…….. 66

4.3.2 MIC/MBC and tolerance determination…… 66

4.3.3 Time-kill activity……... 69

4.3.4 Assessment of biofilm formation…….. 69

4.3.5 ASTM E2149…… 74

4.3.6 Bacterial cell adhesion…….. 77

4.4 Biocompatibility evaluation…… 80

4.4.1 Cell viability and cell membrane integrity assay…….. 80

4.4.2 Cells adhesion and attachments…… 84

4.4.3 Clonogenic survival assay……. 84

4.5 Biochemical profiles……... 87

4.5.1 Estimation of accumulation of intracellular ROS production... 87

4.5.2 Zinc, calcium and phosphorus ion release…… 89

4.5.3 Hoechst and Calcein-AM staining……..... 92

4.6 Gene expression analysis by Real-Time PCR……. 94

4.6.1 Evaluation of expression levels of stress response with NFE2L2, HMOX1 and GADD45α……... 94

4.6.2 Evaluation of inflammation rate with IL-6 and IL-8…… 96

4.6.3 Evaluation of apoptosis level with BAX and BCL-2…… 97

4.7 Protein analysis for NF-kB (p65) expressions…… 97

4.8 Haemocompatibility profiles…….. 99

4.8.1 Full blood count and coagulation analysis…… 100

4.8.2 Haemolysis rate test…….. 102

4.8.3 Whole blood clotting kinetics……... 102

4.8.4 Platelet adhesion…… 105

4.8.5 Whole blood and fibrin attachment……... 105

4.9 Functional time frame of LLDPE nanocomposite films……. 109

4.9.1 *In vitro* degradation in M9 broth……. 109

4.9.2 *In vitro* hydrolytic degradation in PBS solution……. 113

4.9.3 *In situ* soil burial assay……... 115

CHAPTER 5 DISCUSSION…….. 117

5.1 Bactericidal and bacteriostatic status of LLDPE/TiO_2-ZnO nanocomposite films……... 117

5.1.1 Bacteriostatic activity of TiO_2-ZnO nanocomposites under static contact conditions antibacterial activity…….. 117

5.1.2 Bacteriostatic activity of LLDPE/TiO_2-ZnO nanocomposite films guided by ASTM E2149 under dynamic contact conditions antibacterial activity…… 119

5.1.3 Antibacterial mechanisms of LLDPE/TiO_2-ZnO nanocomposite films……. 120

5.2 Bio-interaction of LLDPE/TiO_2-ZnO nanocomposite films at cellular, molecular and protein levels……... 124

5.2.1 Blood and fibroblast cells interaction with LLDPE/TiO_2-ZnO nanocomposite films at cellular level……... 124

5.2.2 Blood and fibroblast cells interaction with LLDPE/TiO_2-ZnO nanocomposite films at genes and protein level……... 129

5.3 Human blood cells interaction with LLDPE/TiO_2-ZnO nanocomposite films…… 134

5.4 Functional time frame of LLDPE/TiO_2-ZnO nanocomposite films…….. 137

5.4.1 Factors affecting the functionality of LLDPE/TiO_2-ZnO nanocomposite films at cellular level…… 142

CHAPTER 6 CONCLUSION AND FUTURE STUDIES…..……. 145

6.1 Conclusion…….. 145

6.2 Future studies……. 148

REFERENCES ……... 149

APPENDICES

LIST OF TABLES

		Page
Table 2.1	The four main groups of HAIs and summary of pathogens responsible for HAIs…….....	8
Table 2.2	List of organisms commonly infecting medical implants and developing biofilms…….....	15
Table 2.3	Diverse application of synthetic polymer in biomedical fields…….....	16
Table 2.4	A comparison of four different types of polyethylene polymer. Structures and common biomedical applications of different polymer properties include differences in branch structure, biomedical applications, density, and melting points. (Adapted from McKeen, 2014)……	18
Table 2.5	Overview of MNPs applications as antibacterial agent. The MNPs embed with polymer nanocomposites as antibacterial agents for biomedical purposes…….....	21
Table 2.6	Standard guidelines used to investigate antibacterial activity of tested materials in different forms purposely designated for biomedical applications……	27
Table 2.7	List of haemocompatibility testing. Its summarised of testing available to evaluate the interactions of blood components with biomaterial-based polymer nanocomposites…….....	34
Table 3.1	Molar extinction coefficients for alamarBlue at different wavelengths……...	45
Table 3.2	List of SBF reagents……..	49
Table 3.3	The RT reaction mixture……	52
Table 3.4	The thermal cycler conditions……...	52
Table 3.5	Sequence of primers used for qPCR…….	53

Table 3.6 Fast thermal cycling conditions for fast plate run on a StepOnePlus™ systems…… 53
Table 3.7 The coagulation, full blood, and differential counts parameters are sent to BP Diagnostic Centre Sdn. Bhd…… 57
Table 4.1 The MIC (mg/mL), MBC (mg/mL) and tolerance level for MDR and non-MDR bacterial HAIs pathogens treated with TiO_2-ZnO nanocomposites in different molar ratio after 24 h treatment periods……... 68
Table 4.2 List of blood parameters for treated LLDPE/TiO_2-ZnO nanocomposite films……..... 101
Table 4.3 Percentage weight loss of the LLDPE/TiO_2-ZnO nanocomposite films after soil burial..…….. 115
Table 4.4 Biodegradable images of the LLDPE/TiO_2-ZnO nanocomposite films prior and after soil burial test…… 116

LIST OF FIGURES

		Page
Figure 2.1	Illustration on HAIs cause significant incidence rates, mortality and excess length of hospital stays. Those outcomes lead to financial burdens for individuals and also for communities in handling HAIs cases (Adapted from Desgupta *et al*. 2015; Zainal Abidin *et al*. 2020; Haque *et al*. 2018). ……	6
Figure 2.2	Percentages of common Gram-positive and Gram-negative bacteria isolated in selected healthcare facilities in 2019. The figure summarises the common isolated bacteria that cause HAIs amongst patients in hospitals in Saudi Arabia (Adapted from Al Mutair *et al*., 2021)……	10
Figure 2.3	Catheter insertion for fluid administration (medication, blood withdrawal or nutritional solutions). Cross-contamination may create possible routes for HAI-causing organisms from the skin microflora of patients or from exogenous microflora from other sources. These organisms directly attach and develop biofilms on catheters, cause HAIs and worsen patient health (Adapted from Crnich, C.J. and Maki, D.G., 2002). ……	14
Figure 2.4	Schematic diagram of visible light induced photocatalytic of TiO_2-ZnO photonic nanocomposites. TiO_2/ZnO nanocomposites performed an excellent photocatalytic and antibacterial activities against both Gram-positive and Gram-negative pathogens (Adapted from Padmavathy and Vijayaraghavan 2008)……..	23
Figure 2.5	*In vitro* biocompatibility assessment to assess cellular and molecular responses to the newly developed polymer based nanocomposites……	32

Figure 3.1 Study workflow for the methodology used in this research. It been divided into four major assays includes antibacterial, cytocompatibility, biochemical, molecular, haemocompatibility and functional time profiles……. 38

Figure 3.2 Hydrolytic degradation of LLDPE/TiO_2-ZnO nanocomposite films. Arrangement of bare LLDPE and LLDPE/25T75Z/5% thin film in PBS solution for 15 weeks……... 62

Figure 3.3 Soil burial assay at the four different site in Malaysia. The photos of four different site location for soil burial assay with GPS coordinate…… 63

Figure 4.1 Antibacterial activity using disk diffusion assay for TiO_2-ZnO nanocomposites against *S. aureus* bacteria under (A) light and (B) dark conditions. Graph of mean inhibition zone diameters from two independent disk diffusion assays with four replicates in each experiments (n=4) showing the antibacterial effect of nanocomposites on the growth of *S. aureus*…… 67

Figure 4.2 Time-kill plots of TiO_2-ZnO nanocomposites against (A) *S. aureus* and (B) MRSA at different molar ratio and time length. Plot of mean log (CFU/mL) from two independent time-kill assays with four replicates in each experiments (n=4) showing the antibacterial effect of nanocomposites on the growth of gram positive bacteria……. 70

Figure 4.3 Time-kill plots of TiO_2-ZnO nanocomposites against (A) *E. coli* and (B) *K. pneumoniae* at different molar ratio and time length. Plot of mean log (CFU/mL) from two independent time-kill assays with four replicates in each experiments (n=4) showing the antibacterial effect of nanocomposites on the growth of gram negative bacteria…… 71

Figure 4.4 Total biofilm mass of (A) *S. aureus* and (B) MRSA obtained from crystal violet assay. Graph of mean biofilm mass of gram positive bacteria treated with TiO_2-ZnO nanocomposites versus untreated bacteria with three replicates in experiments (n=3) showing reduction in biofilm mass. Data represent mean ± standard deviations with significant different (*** $p \leq 0.01$)…… 72

Figure 4.5 Total biofilm mass of (A) *E. coli* and (B) *K. pneumoniae* obtained from crystal violet assay. Graph of mean biofilm mass of gram negative bacteria treated with TiO_2-ZnO nanocomposites versus untreated bacteria with three replicates in experiments (n=3) showing reduction in biofilm mass. Data represent mean ± standard deviations with significant different (*** $p \leq 0.01$)……. 73

Figure 4.6 Antibacterial efficiency of LLDPE/TiO_2-ZnO nanocomposites films with different molar ratios against A) *S. aureus* and B) *E. coli.* Graph of mean reduction percentage of bacteria treated with LLDPE/25T75Z (1,3,5,7 and 10%) nanocomposites films from two independent ASTM E2149 assay with three replicates in each experiments (n=3)…… 75

Figure 4.7 Antibacterial efficiency of LLDPE/25T75Z nanocomposites films with different weight percentages against A) *S. aureus* and B) *E. coli.* Graph of mean reduction percentage of bacteria treated with LLDPE/25T75Z (1,3,5,7 and 10%) nanocomposites films from two independent ASTM E2149 assay with three replicates in each experiments (n=3)…… 76

Figure 4.8 Antibacterial efficiency of LLDPE/TiO_2-ZnO nanocomposites films with different weight percentages against A) *S. aureus* and B) *E. coli.* Graph of mean reduction percentage of bacteria treated with LLDPE/TiO_2-ZnO nanocomposites films from two independent ASTM E2149 assay with three replicates in each experiments (n=3)…… 78

Figure 4.9 FESEM images of bacterial attachments on sample surface after 24 h, 5 days and 7 days. Notes: (A1-A9) SEM morphologies for MRSA; (B1-B9) SEM morphologies for *K. pneumoniae*, respectively for bare and 25T75Z (5 and 10 wt.%) nanocomposites films after 24 h, 5 days and 7 days' incubation treatment…….. 79

Figure 4.10 Cell viability assay (A) and the membrane integrity (B) of HDF cells exposed to LLDPE/TiO_2-ZnO nanocomposite films. Graph of mean cell viability percentage and LDH release of HDF cells treated with LLDPE/TiO_2-ZnO nanocomposites films from two independent assay with three replicates in each experiments (n=3). Results are expressed as mean ± standard deviation with significant results compared with the control (bare) are marked with asterisks (* for $p \leq 0.05$ and ** for $p \leq 0.01$)……. 81

Figure 4.11 Cell viability assay (A) and the membrane integrity (B) of L929 cells exposed to LLDPE/TiO_2-ZnO nanocomposite films. Graph of mean cell viability percentage and LDH release of L929 cells treated with LLDPE/TiO_2-ZnO nanocomposites films from two independent assay with three replicates in each experiments (n=3). Results are expressed as mean ± standard deviation with significant results compared with the control (bare) are marked with asterisks (* for $p \leq 0.05$ and ** for $p \leq 0.01$)……. 82

Figure 4.12 Cell viability assay (A) and the membrane integrity (B) of Kasumi-1 cells exposed to LLDPE/TiO_2-ZnO nanocomposite films. Graph of mean cell viability percentage and LDH release of Kasumi-1 cells treated with LLDPE/TiO_2-ZnO nanocomposites films from two independent assay with three replicates in each experiments (n=3). Results are expressed as mean ± standard deviation with significant results compared with the control (bare) are marked with asterisks (* for $p \leq 0.05$ and ** for $p \leq 0.01$)……. 83

Figure 4.13 Colony formation assay of L929 cells treated on LLDPE/TiO_2-ZnO nanocomposite films surface for eight days. Graph of mean colony-forming unit-fibroblast (CFU-F) treated with LLDPE/TiO_2-ZnO nanocomposites films from two independent assay. Results are expressed as mean ± standard deviation with significant results compared with the control (untreated) are marked with asterisks (* for $p \leq 0.05$ and ** for $p \leq 0.01$)…….. 85

Figure 4.14 FESEM images of HDF cells cultured with LLDPE/TiO_2-ZnO nanocomposite films at 3-days incubation period. The diagrams show cells grown on (A) Bare LLDPE as control, (B) LLDPE/100Z, (C) LLDPE/100T, (D) LLDPE/25T75Z/5% and (E) LLDPE/25T75Z/10% nanocomposite films…… 86

Figure 4.15 Intracellular ROS detection after 48 h treated with LLDPE/TiO2-ZnO nanocomposite films. Graph of mean intracellular ROS production in (A) HDF and (B) Kasumi-1 cell lines exposed to LLDPE/TiO_2-ZnO nanocomposite films from two independent assay. Results are expressed as mean ± standard deviation with significant results compared with the control (untreated) are marked with asterisks (* for $p \leq 0.05$ and ** for $p \leq 0.01$)…….. 88

Figure 4.16 Zinc ion concentration in SBF solution after immersion periods within 28 days. Graph of mean zinc ion released in SBF solution exposed to LLDPE/TiO_2-ZnO nanocomposite films from two independent ICP-OES analysis. Results are expressed as mean ± standard deviation with significant results compared with the control (untreated) are marked with asterisks (* for $p \leq 0.05$ and ** for $p \leq 0.01$)…….. 89

Figure 4.17 Calcium ion concentration in SBF solution after immersion periods within 28 days. Graph of mean calcium ion released in SBF solution exposed to LLDPE/TiO_2-ZnO nanocomposite films from two independent ICP-OES analysis. Results are expressed as mean ± standard deviation with significant results compared with the

control (untreated) are marked with asterisks (* for $p \leq 0.05$ and ** for $p \leq 0.01$)……. 90

Figure 4.18 Phosphorus ion concentration in SBF solution after immersion periods within 28 days. Graph of mean phosphorus ion released in SBF solution exposed to LLDPE/TiO_2-ZnO nanocomposite films from two independent ICP-OES analysis. Results are expressed as mean ± standard deviation with significant results compared with the control (untreated) are marked with asterisks (* for $p \leq 0.05$ and ** for $p \leq 0.01$)…… 90

Figure 4.19 FESEM images of LLDPE/TiO_2-ZnO nanocomposite films after being immersed in SBF solution for 28 days. The diagrams show surface of LLDPE/100Z and LLDPE/25T75Z/5% after immersed in SBF for 28 days…… 91

Figure 4.20 TiO_2-ZnO induces changes in calcein-AM (green images) and Hoechst 33342 (blue staining) staining in fibroblasts cells after being treated for 24 h. Arrows specify the nuclei with chromatin condensation and fragmentation. Images were captured with fluorescence microplate reader with scale bars, 200 μm…… 92

Figure 4.21 Relative expression of genes involved in oxidative stress response mechanism on Kasumi-1 and HDF cell lines. Graph of mean relative expression of (A) Kasumi-1 and (B) HDF cell lines exposed to bare LLDPE, LLDPE/25T75Z/5% and LLDPE/25T75Z/10% from two independent qPCR runs with four replicates in each assay. Results are expressed as mean ± standard deviation with significant results compared with the control (untreated) are marked with asterisks (* for $p \leq 0.05$ and ** for $p \leq 0.01$)……. 95

Figure 4.22 Relative expression of genes involved in inflammation response mechanism on Kasumi-1 and HDF cell lines. Graph of mean relative expression of (A) Kasumi-1 and (B) HDF cell lines exposed to bare LLDPE, LLDPE/25T75Z/5% and

LLDPE/25T75Z/10% from two independent qPCR runs with four replicates in each assay. Results are expressed as mean ± standard deviation with significant results compared with the control (untreated) are marked with asterisks (* for $p \leq 0.05$ and ** for $p \leq 0.01$)…….. 96

Figure 4.23 Relative expression of genes involved in apoptosis response mechanism on Kasumi-1 and HDF cell lines. Graph of mean relative expression of (A) Kasumi-1 and (B) HDF cell lines exposed to bare LLDPE, LLDPE/25T75Z/5% and LLDPE/25T75Z/10% from two independent qPCR runs with four replicates in each assay. Results are expressed as mean ± standard deviation with significant results compared with the control (untreated) are marked with asterisks (*for $p \leq 0.05$ and ** for $p \leq 0.01$)…….. 98

Figure 4.24 Immunoblot analysis of selected proteins involved in inflammation and immune response. The studied protein samples were obtained from bare LLDPE, LLDPE/25T75Z/5% and LLDPE/25T75Z/10% in two independent assay. Differential protein expressions of NF-κB (p65) was expressed in Kasumi-1 and HDF cells grown on the study materials for 48 h. β-actin protein profile was used as a loading control. Only one representative result is presented……. 99

Figure 4.25 Effects of LLDPE/TiO_2-ZnO nanocomposite films on APTT human plasma. Graph of mean APTT (s) treated with bare LLDPE and LLDPE/25T75Z/5% and LLDPE/25T75Z/10% in three independent assay. Results are expressed as mean ± standard deviation with significantF results compared with the control (untreated) are marked with asterisks (*for $p \leq 0.05$ and ** for $p \leq 0.01$)……. 100

Figure 4.26 LLDPE/TiO_2-ZnO nanocomposite films effect on hemolysis assay. (A) Graph of mean percentage of hemolysis induced by bare LLDPE, LLDPE/25T75Z/5% and LLDPE/25T75Z/10% in two independent assay with four replicates in each experiment (n=4). Results are expressed as mean ± standard deviation with significant results compared with the control (Triton X-100) are marked with asterisks (*for $p \leq 0.05$ and ** for $p \leq 0.01$). (B) Visual inspection of the tubes containing diluted total blood after exposure to LLDPE/TiO_2-ZnO nanocomposite films……. 103

Figure 4.27 Whole blood clotting kinetics of LLDPE/TiO_2ZnO nanocomposite films. Graph of mean blood clotting time indicated at OD540 nm induced by bare LLDPE, LLDPE/25T75Z/5% and LLDPE/25T75Z/10% in two independent trials……. 104

Figure 4.28 LLDPE/TiO_2-ZnO nanocomposite films effect on platelet adhesion. The nanocomposite films were stained with calcein AM for 30 min; (A) Bare LLDPE, (B) LLDPE/25T75Z/5% and (C) LLDPE/25T75Z/10% film. The adherent platelet treated on LLDPE nanocomposite films for 1 h surface was observed by Calcein AM staining; (A) Bare LLDPE, (B) LLDPE/25T75Z/5% and (C) LLDPE/25T75Z/10% film…….. 106

Figure 4.29 The effect of LLDPE/TiO_2-ZnO nanocomposite films on washed human RBCs. The effect of (A) bare LLDPE, (B) LLDPE/25T75Z/5% and (C) LLDPE/25T75Z/10% nanocomposite films on RBCs as observed with FESEM after 1 h exposure. In LLDPE with TiO_2-ZnO LLDPE nanocomposite films, singular echinocytes (Yellow arrow) and stomatocytes (Red arrow) were observed…… 107

Figure 4.30 The effect of LLDPE/TiO_2-ZnO nanocomposite films on PRP. FESEM images of the platelet adhesion/activation and thrombus formation on LLDPE/TiO_2ZnO nanocomposite films for 1 h…….. 108

Figure 4.31 Optical density at 600 nm of *P. aeruginosa* bacterial suspension treated with bare LLDPE and LLDPE/25T75Z/5% nanocomposite films. Graph of *P. aeruginosa* bacterial growth after being treated with bare LLDPE and LLDPE/25T75Z/5% nanocomposite films for four weeks with addition of glucose in M9 broth in one independent trial. …… 110

Figure 4.32 Optical density at 600 nm of *P. aeruginosa* bacterial suspension treated with bare LLDPE and LLDPE/25T75Z/5% nanocomposite films. Graph of *P. aeruginosa* bacterial growth after being treated with bare LLDPE and LLDPE/25T75Z/5% nanocomposite films for four weeks without addition of glucose in M9 broth in one independent trial…….. 110

Figure 4.33 The weight loss of treated LLDPE/TiO_2-ZnO nanocomposite films after 30 days. Graph of percentage reduction in weight of bare LLDPE and LLDPE/25T75Z/5% in two different culture systems at one independent experiment……. 111

Figure 4.34 FESEM images of LLDPE/TiO_2-ZnO nanocomposite films after being immersed in M9 broth for 30 days. *In vitro* biodegradation evaluation of bare LLDPE and LLDPE/25T75Z/5% nanocomposites films in M9 broth with and without glucose as additional nutrient…… 112

Figure 4.35 The responsive pH of PBS solution and percentage weight remaining of LLDPE/TiO_2-ZnO nanocomposite films for 15 weeks. Graph of pH changes versus time growth after being treated with bare LLDPE and LLDPE/25T75Z/5% nanocomposite films. (B) Graph of reduction in weight of bare LLDPE and LLDPE/25T75Z/5% nanocomposite films being immersed in PBS solution for 15 weeks in one independent trial……. 113

Figure 4.36 FESEM images of LLDPE/TiO_2-ZnO nanocomposite films after being immersed in PBS solution for 15 weeks. Hydrolytic biodegradation activity of bare LLDPE and LLDPE/25T75Z/5% nanocomposites films in PBS solution…….. 114

Figure 5.1 Antibacterial mechanism of LLDPE/TiO_2-ZnO nanocomposites films against gram positive and gram negative pathogens. It showed the ROS and free radicals generated from polymer films induced oxidative stress in cells. The Zn^{2+} ions released directly adhered on teichoic acid, LPS layer and cell walls of bacteria leading to cell death…….. 123

Figure 5.2 Uncontrolled intracellular and extracellular ROS generation associated with NP exposure. The generation of ROS may disturb the metabolic process through electron transport chains, NADPH oxidant, cytokines and growth factor receptors. By contrast, the induction of extracellular factors is commonly associated with free radicals, inflammation and genotoxic risk…… 125

Figure 5.3 The schematic illustration of NF-kβ signalling pathway involved in cell interaction with LLDPE/TiO_2-ZnO nanocomposite films. This mechanism was predicted based on HDF and Kasumi-1 cell line models. As highlighted in this study, the ROS generation induced oxidative stress in cells. Thus, it alters the inflammation genes and proteins involved in NF-kβ signalling pathway…… 133

Figure 5.4 Illustration of LLDPE nanocomposite films with bloodstream components in vein. Blood is a complex organ which comprising of 55% plasma, 44% erythrocytes, and 1% leukocytes and platelets (Weber *et al*. 2018)…….. 134

Figure 5.5 Microorganisms involved in polymer biodegradation studies in different area. Locally isolated microbial strains have been identified in different sites for degradation. …….. 139

LIST OF UNITS AND SYMBOLS

°C	Degree Celsius
e−	Electrons
g	Gram
H_2O_2	Hydrogen peroxide
·OH	Hydroxyl radicals
h	Hour
h+	Hole
KV	Kilovolt
mL	Milliliter
µM	Micrometer
µL	Microliter
%	Percentage
rpm	Revolutions per minute
sec	Second
$O_2 \bullet^-$	Superoxide
T	Titanium dioxide
V	Volt
Zn^{2+}	Zinc ions
Z	Zinc oxide

LIST OF ABBREVIATIONS

A. baumanii	*Acinetobacter baumanii*
AB	Alamar blue
AML	Acute myeloid leukaemia
APTT	Activated Partial Thromboplastin Time
ASTM	American Society for Testing and Materials
BAX	BCL2 Associated X, BAX- alpha
BCL-2	B-cell lymphoma 2
BSA	Bovine serum albumin
CAUTI	Catheter-associated urinary tract infections
cDNA	Complementary DNA
C. freundii	*Citrobacter freundii*
CLABSI	Central line-associated bloodstream infections
CLSI	Clinical and Laboratory Standard Institute
CM-H_2DCFDA	2, 7-dichlorodihydrofluoresce in diacetate acetyl ester
CV	Covalent band
$CaCl_2$	Calcium chloride
DMEM/F-12	Dulbecco's Modified Eagle's Medium/Nutrient Mixture F-12 Ham
DMSO	Dimethyl sulfoxide
E. coli	*Escherichia coli*
E. faecalis	*Enterococcus faecalis*
EDTA	Ethylenediaminetetraacetic acid
ELISA	Enzyme-linked immunosorbent assay
EPS	Extracellular polymer substances
FBS	Fetal bovine serum
FDA	American Food and Drug Administration
FPA	Fibrinopeptide A
FESEM	Field Emission Scanning Electron Microscope

GADD45A	Growth arrest and DNA damage-induced 45 A
GAPDH	Glyceraldehyde 3-phosphate dehydrogenase
GRAS	Generally Recognised as Safe
HAIs	Healthcare-associated infections
Hb	Hemoglobin
HDF	Human dermal fibroblast
HDPE	High-density polyethylene
HEPES	N-2-hydroxyethylpiperazine-N-ethanesulfonic acid
HMOX1	Heme Oxygenase 1
ICP-OES	Inductively Coupled Plasma Optical Emission spectroscopy
IL-6	Interleukin 6
IL-8	Interleukin 8
ISO	International Organisation for Standardisation
K.pneumoniae	*Klebsiella pneumonia*
KCL	Potassium chloride
$K_2HPO_4.3H_2O$	Potassium phosphate dibasic trihydrate
L929	Mouse fibroblast
LB	Luria-bertani
LDH	Lactate dehydrogenase
LDPE	Low-density polyethylene
LLDPE	Linear low density polyethylene
LPS	Lipopolysaccharides
M. morganii	*Morganella morganii*
M9	M9 minimal medium
MBC	Minimum bactericidal concentration
MCH	Mean Corpuscular Hemoglobin
MCHC	Mean Corpuscular Hemoglobin Concentration
MCV	Mean Cell Volume
MDR	Multi drug resistant
MDPE	Medium-density polyethylene
MIC	Minimum inhibitory concentration

MNPs	Metal-oxide NPs
MRSA	methicillin-resistant *Staphylococcus aureus*
MSSA	methicillin-susceptible *Staphylococcus aureus*
$MgCl_2.6H_2O$	Magnesium chloride hexahydrate
NF-kβ	Nuclear Factor kappa-light-chain-enhancer of activated B cells
NFE2L2	Nuclear factor erythroid 2-related factor 2
NO	Nitric oxide
NPs	Nanoparticles
$NaCl_2$	Sodium chloride
$NaHCO_3$	Sodium bicarbonate
Na_2SO_4	Sodium sulfate
OD	Optical density
OHP	Overall hemostasis potential
P. aeruginosa	*Pseudomonas aeruginosa*
P. mirabilis	*Proteus mirabilis*
P. vulguris	*Proteus vulguris*
P25	Pure titanium dioxide
PANI	Polyaniline
PBS	Phosphate buffer saline
PCR	Polymerase chain reaction
PEG	Polyethylene glycol
PP	Polypropylene
PPP	Platelet poor plasma
PRP	Platelet rich plasma
PT	Prothrombin time
PVC	Packed cell volume
PVC	Poly(vinyl chloride)
qPCR	quantitative Polymerase Chain Reaction
R. dentocariosa	*Rothia dentocariosa*
RBC	Red blood cell
RDW	Red Cell Distribution Width

RIPA	Radioimmunoprecipitation assay
RNA	Ribonucleic acid
ROS	Reactive oxygen species
RPMI	Roswell Park Memorial Institute
S. aureus	*Staphylococcus aureus*
S. epidermidis	*Staphylococcus epidermidis*
S. maltophilia	*Stenotrophomas maltophilia*
S. maresecens	*Serratia maresecens*
S. mitis	*Streptococcus mitis*
S. mucilaginous	*Stomatococcus mucilaginous*
S. salivarius	*Streptococcus salivarius*
S. sobrinus	*Streptococcus sobrinus*
S. viridans	*Streptococcus viridans*
SBF	Simulated body fluid
SDS-PAGE	Sodium dodecyl sulfate-polyacrylamide gel electrophoresis
SSI	Surgical site infections
TAT	Thrombin–antithrombin complex
TBST	Tris-Buffered Saline and Tween 20
TTIP	Titanium isopropoxide
VAP	Ventilator-associated pneumonia
VB	Valence band
WBC	White blood cell
WHO	World Health Organisation

LIST OF APPENDICES

Appendix A Human ethic approval

Appendix B List of publications

Appendix C Academic award and intellectual property

KAJIAN KEBIOSERASIAN DAN KETOKSIKAN NANOKOMPOSIT POLIMER TIO_2 –ZNO HETEROGENUS DENGAN AKTIVITI BAKTERISIDAL DIPERTINGKATKAN

ABSTRAK

Jangkitan berkaitan penjagaan kesihatan adalah isu keselamatan yang diberi perhatian utama sedunia sebagai penyumbang kepada kadar kematian dalam kalangan pesakit disebabkan oleh patogen yang berkait langsung dengan permukaan polimer bioperubatan yang tercemar dari alat perubatan yang tertempat atau implant. Polimer nanokomposit telah menjadi potensi penyelesaian bagi HAI disebabkan oleh cara tindakbalas spesies oksigen reaktif (ROS) dan radikal bebas. Dalam seksyen pertama, kajian ini menghuraikan potensi bakteriostatik dan bakterisidal lapisan-lapisan nipis polimer nanokomposit terhadap pathogen-patogen HAI, termasuklah strain-strain tahan pelbagai ubat (MDR) dan bukan MDR. Dalam seksyen kedua, analisis awal tindak balas biointeraksi *in vitro* pada model-model sel selanjar fibroblas dan darah menunjukkan tanda-tanda gangguan integriti membran sel, yang mungkin disebabkan oleh aktiviti radikal bebas seperti pembebasan intrasel ROS dan ion Zn (Zn^{2+}) ketika proses penyesuaian selular awal terhadap lapisan nipis polimer nanokomposit TiO_2–ZnO. Kajian tahap molekul terdahulu mendedahkan interaksi antara sel dan lapisan nipis polimer nanokomposit mungkin mencetuskan tekanan oksidatif dan mekanisma pro-radang melalui lata utama faktor nuklear-κB. Kajian lanjutan menemukan sel yang mampu mengekalkan potensi daya maju dan klonogenik serta terlibat dalam laluan anti-apoptosis. Dapatan kajian mencadangkan tindak balas tekanan oksidatif sementara oleh lapisan nipis

polimer nanokomposit terhadap sel yang dirawat serta tidak membahayakan sel. Tambahan pula, lapisan-lapisan nipis polimer nanokomposit ini didapati dapat menyebabkan hemokompatibliti yang baik dengan lekatan dan pengaktifan platelet yang minimum, sehingga mengurangkan pembentukan trombus mengikut garis panduan Bahagian 4-ISO 10993. Kesimpulannya, lapisan nipis polimer nanokomposit TiO_2–ZnO mampu menjadi polimer bioperubatan yang berpotensi terhadap HAI yang memaparkan sifat-sifat hemokompatibiliti dan aktiviti-aktiviti bakterisidal yang dipertingkat terutamanya strain-strain MDR. Kajian menyeluruh terhadap interaksi radikal bebas dan mekanisme homeostasis molekul adalah perlu untuk lebih memahami tindak balas tekanan oksidatif sementara oleh lapisan nipis polimer nanokomposit terhadap sistem manusia.

BIOCOMPATIBILITY AND TOXICITY STUDIES OF HETEROGENEOUS TIO_2-ZNO POLYMER NANOCOMPOSITE WITH ENHANCED BACTERIAL ACTIVITY

ABSTRACT

Healthcare-associated infections (HAIs) are a major safety concern globally as they contribute to mortality rates amongst patients due to pathogens from direct contact with a contaminated biomedical polymer surface from the indwelling or implanted medical devices. Polymer nanocomposites have become a promising solution for HAIs owing to reactive oxygen species (ROS) and free radicals' mode of action. In the first section, this work revealed the bacteriostatic and bactericidal potentials of TiO_2–ZnO polymer nanocomposite films against HAI pathogens, including multidrug-resistant (MDR) and non-MDR strains. In the second section, the initial analysis of the *in vitro* bio-interaction responses on fibroblast and blood cell line models showed signs of cell membrane integrity disturbance, which might be due to free radicals' activities, such as the release of intracellular ROS and Zn ions (Zn^{2+}) during the initial cellular adaptation process on the TiO_2–ZnO polymer nanocomposite film. Molecular studies revealed that the cell–polymer nanocomposite film interaction possibly triggered the oxidative stress and pro-inflammatory mechanisms through the principal cascades of Nuclear Factor-κB. Further analysis found that cells could maintain the viability and clonogenic potential and were involved in the anti-apoptosis pathway. Findings suggested the transitory oxidative stress responses of polymer nanocomposite films towards treated cells and not harmful to the cells. Furthermore, these polymer nanocomposite films were found and could

render good haemocompatibility with minimal platelet adhesion and activation, thereby reducing the thrombus formation according to the ISO 10993-Part 4 Guidelines. In conclusion, TiO_2–ZnO polymer nanocomposite films could present as a promising biomedical polymer against HAIs that displayed biocompatibility properties and enhanced bactericidal activities especially MDR strains. Comprehensive work on free radicals' interaction and molecular homeostasis mechanism is needed to further understand the transitory oxidative stress responses of polymer nanocomposite films towards human systems.

CHAPTER 1

INTRODUCTION

1.1 Research background

Hospital-associated infections (HAIs) or nosocomial infections is globally known as one of the leading complications related with indwelling medical devices. It is an infections acquired during health treatment (Monegro *et al.* 2020; Sikora and Zahra, 2020). HAIs manifest within 48 h or more after hospital admission and can also appear within 30 days after patient discharge (WHO 2021; Leaper and Edminston 2017; Revelas 2012). There are about 4% of patients in U.S. hospitals involved with HAIs in 2011 and most commonly are directly associated with prolonged hospitalisation and thus increase healthcare costs contributing to the financial burden.

Central line associated bloodstream infections (CLABSI) and catheter-related bloodstream infection (CRBSI) is the commonest cause of HAIs, which the complications arising due to the bacterial colonization of medical appliances such as peripheral intravascular (IV) and central venous catheters used in patients after certain periods. It is estimated that approximately 80,000 cases occurred per year in the United States of America (USA) (O'Grady *et al*. 2011). Also, the incidence of CRBSI alone in the hospitals shown to be 1.1 to 5.5 episodes per 1000 catheter days and mostly causes mortality among patients (Ravani *et al*. 2013). The significant incidence of such infection origin from the fact that the insertion into patients provide an ideal environment for bacterial attachment and growth leading to the biofilm formation (Danese, P.N., 2002).

Biomaterial is defined as any type of engineered material being used in medical fields which is pharmacologically inert and safe to be used in living systems (Park 2012). It also should reliable to be used in targeted period of applications to facilitate and improving current health systems. The used of biomaterial as indwelling or implanted devices has risen due to the greater incidences of cross contamination and the development of drug resistant bacterial strains on biomedical appliances. As the indwelling catheters been infected with bacterial biofilms, it makes the antibiotic therapies less effective. Thus, alternative strategies are urgently needed to overcome HAIs issues.

Recently, nanotechnological approaches, such as the incorporation of metal oxide nanoparticles (MNPs) into polymer matrix, have been used by scientist to develop efficient antibacterial agents against MDR and non-MDR pathogens. Deposition of MNPs such as Ag, Ti, TiO_2 and ZnO shown antibacterial potential by inhibit the bacterial adhesion on catheters has been reported in previous studies (Sánchez *et al*. 2021; Vaitkus *et al*. 2021; Zhang *et al*. 2019; Galiano *et al*. 2008; Samuel and Guggenbichler 2004). In recent decades, many attempts have been made by researchers to modify the catheter surface with the MNPs (Park *et al*. 2002; Srinivasan *et al*. 2006). However, there still no coated catheters that are effective for the treatments are commercially available. Previous study showed the silver-coated urinary catheter potentially to reduce HAIs infection however had insignificant effect after being used for longer periods due to the development of sticky mucoid biofilm (Verleyen *et al*. 1999; Thibon *et al*. 2000).

The proposed strategy of adding two MNPs into polymer nanocomposites has greater potential application for antibacterial surfaces in biomedical devices compared with the use of individual MNPs to combat a wide range of bacteria involved in HAIs especially MDR pathogens. Although TiO_2–ZnO has great antibacterial activities, studies on the reactive oxygen species (ROS), free radical ions and metal ions released from TiO_2–ZnO embedded in polymer nanocomposites, especially their impact on human systems, are very limited. ROS have advantages in antibacterial therapy against most Gram-positive and Gram-negative organisms, including MDR pathogens. However, the overaccumulation of ROS in cells could disturb the equilibrium between ROS (Memar *et al.*, 2018; Lushchak, 2011). Uncontrolled ROS release is involved in cellular homeostatic imbalance and baneful implication to human systems (Snezhkina *et al.*, 2019). Therefore, the present study aimed to assess the antibacterial potential and safety of TiO_2–ZnO polymer nanocomposite on various cell lines.

1.2 Research objectives

1.2.1 General Objective

To determine the antibacterial, biocompatibility, haemocompatibility and toxicity studies of TiO_2–ZnO polymer nanocomposite films for biomedical application.

1.2.2 Specific Objectives

1. To access the antibacterial profiles of the TiO_2–ZnO polymer nanocomposite films against Gram-positive and Gram-negative bacteria panels by using comprehensive antibacterial studies.

2. To evaluate the biocompatibility profiles of TiO_2–ZnO polymer nanocomposite films involving cell viability assay, membrane integrity and clonogenic profiles.
3. To analyse the biochemical activities and releasing of metal ion profiles in simulated body fluid (SBF) and ROS from TiO2–ZnO polymer nanocomposite films.
4. To investigate the haemocompatibility profiles of TiO_2–ZnO polymer nanocomposite films using human blood guided by ISO 10993-4.
5. To understand the molecular interaction of TiO_2–ZnO polymer nanocomposite films with human skin and blood cell lines.
6. To determine the functional time profiles of TiO_2–ZnO polymer nanocomposite films under four analysis includes *in situ* functional time frame, *in vitro* biodegradation studies, hydrolytic degradation and leaching test in SBF solution.

CHAPTER 2

LITERATURE REVIEW

2.1 Biomedical devices and healthcare-associated infections

The burden of HAIs worldwide, especially in Asia, is unknown owing to the lack of surveillance systems. Approximately 25% of hospitalised patients have high HAI risk, which is about 2–20 times the HAI risk in developed Asia-Pacific countries (Ling *et al.* 2015). The prevalence of HAIs in Malaysia increased from 18% in 2016 to 19.8% in 2017 (Zainol Abidin *et al*. 2020). Other developed countries, such as the USA and Europe, have HAI incidence density between 13.0 and 20.3 cases amongst 1000 patients per day (Allegranzi *et al.* 2011). HAI is one of the top 10 causes of mortality amongst hospitalised patients in the US (AHRQ, 2021). HAIs are also associated with healthcare costs of $28 billion to $33 billion and €7 billion annually in the US and Europe (Sikora and Zahra, 2020).

Studies suggested increased mortality in patients with cardiac surgery, respiratory tract infections and ICU-acquired bloodstream infections, who are highly prone to be infected with MDR and non-MDR HAI organisms. Crude mortality for patients with HAIs who underwent surgery is remarkably higher (15.4%) compared with patients who did not develop HAIs (5.7%) (Massart *et al*. 2020). Other international study showed that older patients in the ICU have considerably high crude excess mortality (Rosenthal *et al*. 2010). HAIs shown increase in financial burden due to those factors illustrated in Figure 2.1.

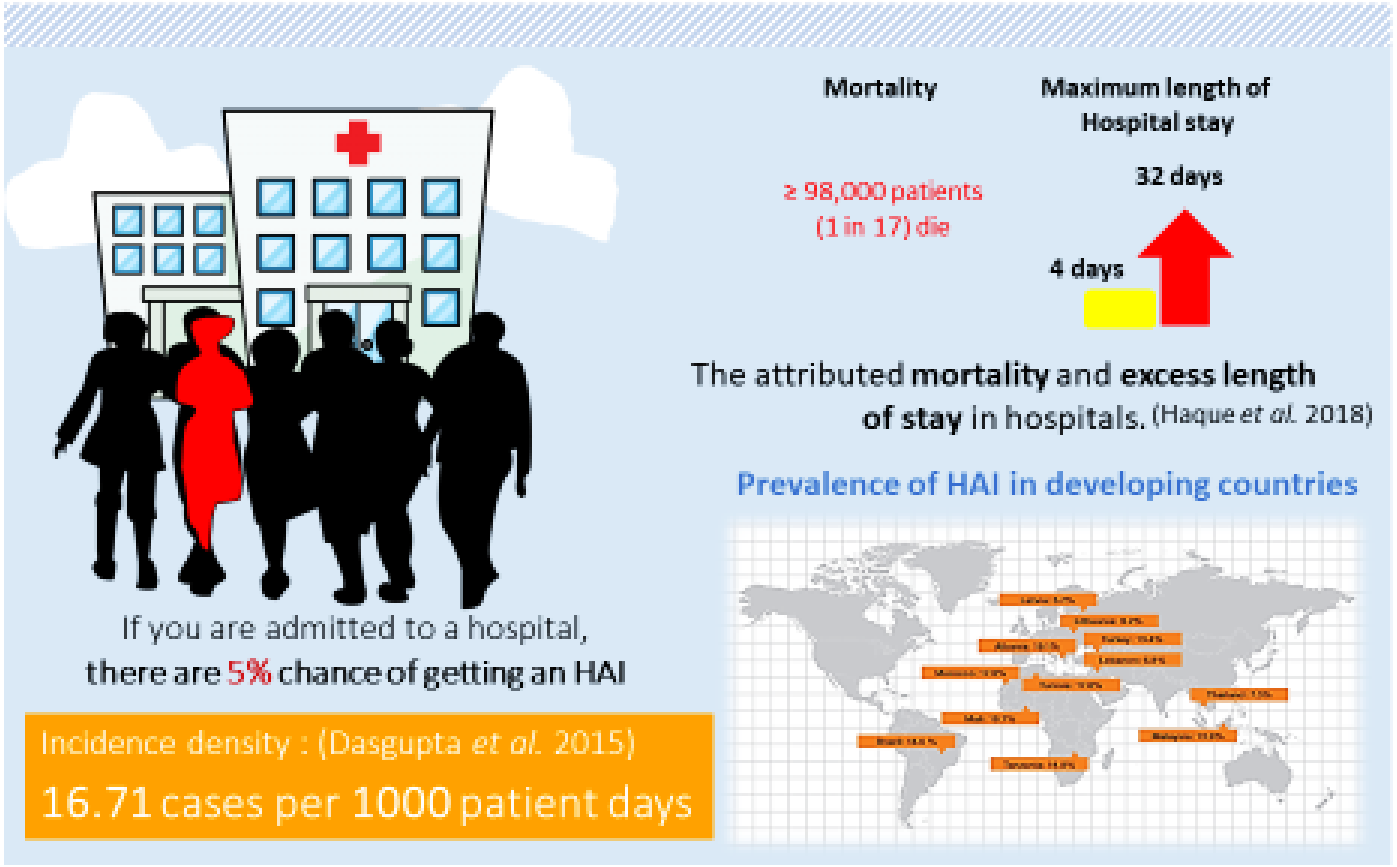

Figure 2.1 **Illustration on HAIs cause significant incidence rates, mortality and excess length of hospital stays.** Those outcomes lead to financial burdens for individuals and also for communities in handling HAIs cases (Adapted from Desgupta *et al*. 2015; Zainal Abidin *et al*. 2020; Haque *et al*. 2018).

The two HAI transmission routes are by endogenous (self-infection) or exogenous (cross-infection) transmission from person to person or through the healthcare setting, such as ventilator, medical equipment or device contamination and food contamination (Soussan *et al.* 2019; Santajit *et al* 2016). HAIs related to device usage or equipment insertion contribute to the increase in mortality rates to 25%–38% (Mathur *et al.* 2021). HAIs also can be contracted by patients after direct contact with contaminated surface, undergoing surgeries or medical treatments or inhaling aerosol droplets from infected patients (Bonilla-Gameros *et al.* 2020; Khan *et al*. 2015).

HAIs can be divided into 13 groups with 50 different infections sites, specifically along the urinary tract, surgical and soft tissues, stomach and intestines and respiratory system (Raka *et al*. 2006). The National Healthcare Safety Network with Centre for Disease Control (CDC) surveillance has classified HAIs into four main groups: central line-associated bloodstream infections (CLABSI), catheter-associated urinary tract infections (CAUTI), surgical site infections (SSI) and ventilator-associated pneumonia (VAP). The responsible HAI pathogens for each group is summarised in Table 2.1. Most HAI pathogens are associated with the patients' endogenous flora; however, cross-infection via infected persons may worsen patient health.

Table 2.1 Summary of the four main groups of HAIs and the pathogens responsible for HAIs.

Group	Microorganisms	References
Central line-associated bloodstream infections (CLABSI)	Gram positive: *Staphylococcus aureus,* Methicillin-resistant *Staphylococcus aureus, Enterococcus spp.,* Coagulase-negative *staphylococci.* Gram negative: *Enterobacteriaceae, Citrobacter spp., Enterobacter spp., Escherichia coli, Klebsiella spp., Proteus spp., Serratia marcescens*	Lin *et al*. 2017
Catheter-associated urinary tract infections (CAUTI)	Gram positive: *Enterococcus faecalis, Vancomycin-resistant enterococci, Streptococcus.* Gram negative: *E. coli, Pseudomonas spp., Proteus mirabilis, Enterobacter spp., Citrobacter spp., Klebsiella spp., Acinetobacter, E. faecalis*	Zahran *et al*. 2019
Surgical site infections (SSI)	Gram positive: *S. aureus,* Coagulase-negative *staphylococci, Streptococci, Enterococci* Gram negative: *Bacilli, Acinetobacter ssp., E. coli, Proteus, Klebsiella ssp.*	Mukagendaneza *et al*. 2019
Ventilator-associated pneumonia (VAP)	Gram positive: MRSA, Coagulase-negative *Staphylococci, S. aureus.* Gram negative: *Acinetobacter baumanii, Pseudomonas aeruginosa, Stenotrophomas maltophilia, Klebsiella pneumonia, Serratia maresecens, Citrobacter freundii, E. coli, Morganella morganii, Proteus vulguris.*	Thakuria *et al*. 2013

2.1.1 Multidrug resistant and non-multidrug resistant HAIs pathogen issues

According to Al Mutair *et al.* (2021), 29,393 types of pathogens isolated in the ICU (41.7%), wards (32.1%) and outpatient (26.2%) cause HAIs within 5 years (2015–2019). The Gram-positive and -negative bacteria that caused HAIs in 2019 are summarised in Figure 2.2. Gram-negative bacteria are frequently associated with HAIs (76.4%) compared with Gram-positive bacteria (20.2%). Another review reported that *Staphylococcus aureus* (*S. aureus*) (30.06%) is the most common pathogen isolated at the surgical site, followed by *Escherichia coli* (*E. coli*) (19.73%), *Klebsiella* species (17.27%) and coagulase-negative *Staphylococci* (CONS, 12.43%) (Birhanu and Endalamaw, 2020). Another study reported the same burden of bacterial pathogens, in which *S. aureus* (30.4%) has the highest percentage amongst other isolated pathogens, followed by CONS (11.7%), *E. coli* (9.4%), *Enterococcus faecalis* (*E. faecalis*) (5.9%), *Pseudomonas aeruginosa* (*P. aeruginosa*) (5.5%), *Enterobacter* species (4.0%) and *Klebsiella* species (4.0%) (WHO, 2016).

MDR pathogens are recognised as an important cause of HAIs, particularly amongst immune-compromised patients. Methicillin-resistant *S. aureus* (MRSA) infection is the most common contributor to Malaysia's HAI cases because of their resistance towards existing antibiotics (Zainol Abidin *et al*. 2020). According to Neubeiser *et al.* (2020), 31,052 patients suffer from HAIs per year and 6.87% of them die from HAIs. They also found that MRSA (51.3%) is the most common isolated pathogen in deceased patients in hospitals in Germany.

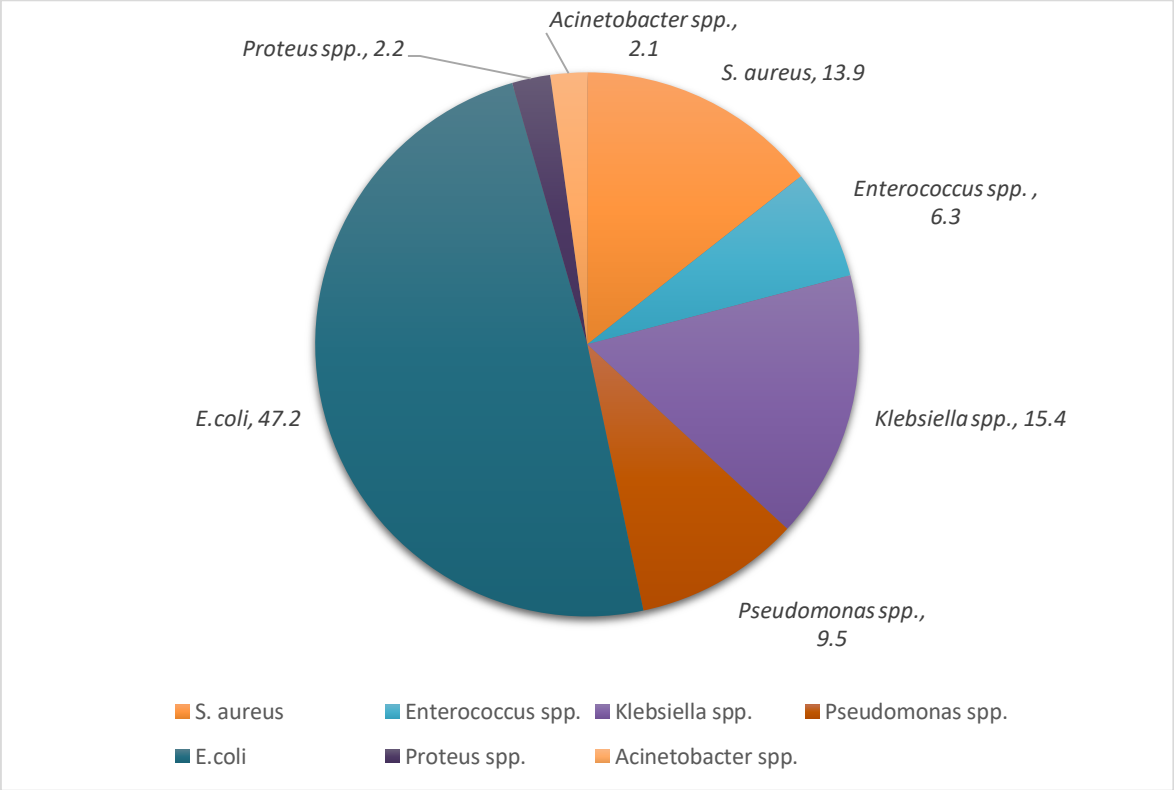

Figure 2.2 **Percentages of common Gram-positive and Gram-negative bacteria isolated in selected healthcare facilities in 2019.** The figure summarises the common isolated bacteria that cause HAIs amongst patients in hospitals in Saudi Arabia (Adapted from Al Mutair *et al.*, 2021).

Antibiotic resistance is the capability of Gram-positive and Gram-negative bacteria to resist specific antibiotics that were previously used in treatments. MDR pathogens develop antibiotic resistance within 90 days after the intravenous administration of antibiotics (Kalil *et al*. 2019). Several factors, such as patients' lack of discipline to follow the given prescription and take the correct dosage at the specified time, may also lead to antibiotic resistance. Doctors need to increase antibiotic usage when new resistance mechanisms develop from MDR pathogens. Therefore, the effectiveness of existing HAI treatments weakens and results in limited treatment alternatives, prolonged hospitalisation and increased healthcare resour[p;l.,ce use (Sehmi *et al*. 2016).

These factors will increase the development of resistant bacterial strains and the risk of death amongst patients. Several preventive measures are performed in healthcare settings to minimise HAI risks. The CDC (Centers for Disease Control and Prevention) has issued guidelines for practises, such as conscientious hygiene procedures, rigorous cleaning, sterilisation and disinfection, and designed organisational and administrative measures (Aljamali *et al*. 2020; Percival *et al*., 2014; Mehta *et al*. 2014). Yet, the control measures for HAI transmission is still weak, especially in the environmental aspect.

Abundant sterilisation and disinfection techniques, such as the use of bleach, quaternary ammonium compounds, UV light and hydrogen peroxide vapour, are available. However, these strategies still have their own limitations. The sensitivity of bacteria to disinfectant, the lengthy time required for sterilisation procedures, and expensive costs limit the frequency of usage of these strategies in most hospitals. Time and training are required to instil the importance of keeping a clean environment to patients and cleaning staff, who are the frontline of environment disinfection (Shafer and Cox, 2014). Therefore, engineering polymer-based nanocomposites on the surface of biomedical devices can enhance material properties to reduce bacterial contamination and HAI risks.

2.1.2 Biofilm development issues related to medical devices

The major concerns for the failure of indwelling and implant devices are bacterial biofilm formation and colonisation (Mirzaei *et al*. 2020; Veerachamy *et al*., 2014). The management of biofilm colonisation for the prevention of device-associated infections and HAIs is a critical issue because antibiotic therapy is ineffective against MDR HAI pathogens. Biofilms contribute about 65% of HAIs (Malheiro and Simões, 2017).

The three common aetiological agents of HAIs that form biofilms include *Staphylococci* species (*S. aureus* and *Staphylococcus epidermidis* (*S. epidermidis*)), *E. coli* and *P. aeruginosa* (Kranjec *et al*. 2021). Previous study indicated *S. aureus* cause a remarkable increase in the mortality rates amongst patients with coinfections, especially those infected with CAUTIs (Todd and Peter, 2019). Most hospitalised patients (15%–25%) are inserted with indwelling urinary catheters. The prolonged use of catheters for more than 30 days' results in 100% bacterial colonisation on catheters (Delcaru *et al*. 2016). Other indwelling medical devices, such as heart devices and orthopaedic implants, are also prone to biofilm colonisation (Verderosa *et al*. 2019).

A biofilm is an organised multimicrobial sessile community that grows in a matrix of extracellular polymer substances (EPSs) produced by bacteria as a protective barrier from antibacterial agent molecules and host immune responses (Vestby *et al*. 2020; Bjarnsholt, 2011). The three main stages of biofilm formation are adhesion, colonisation and maturation (Pintucci *et al*. 2010). Bacterial cells irreversibly adhere to each other, which results in a rapid alteration in the expression of several genes responsible for EPS and the formation of biofilm layers on device surfaces (Gupta *et al*. 2016; Irie *et al*. 2012; Flemming and Wingender 2010).

EPS is consist of a complex biochemical mixture of biomolecules, such as polysaccharides, proteins, glycopeptides, lipids and nucleic acids. Moreover, EPS exhibits viscoelastic behaviour, which allows biofilms to resist mechanical stress in its surrounding and become stable (Kostakioti *et al*. 2013). The third maturation stage, which leads to the development of antibiotic resistance, starts as the biofilm thickness increases.

Once the biofilm matures, plankton microorganisms disperse into the surrounding environments. The detached cells will disseminate to new target surfaces and start to produce new sessile populations on devices.Ramasamy and Lee (2016) and Taylor *et al.* (2012) found that the effectiveness of antibiotics is reduced and inactivated by multiple binding to biomolecule components in EPS and by nutrients in biofilm. Treating biofilms is challenging because of the lack of biomarkers, and the bacteria that cause biofilm formation are difficult to identify upon entry into the body (Paharik *et al*. 2016).

HAIs are usually initiated by medical devices implanted in the body, such as catheters, as shown in Figure 2.3. HAIs can also occur because of other reasons, such as contaminated disinfectants; infections from the surgical theatre, surgical equipment, surgeon or clinical staff or other patients in the hospital and distant local infections (Veerachamy *et al*. 2014; Francolini and Donelli, 2010). Gram-positive and Gram-negative bacteria can develop biofilms on medical devices as tabulated in Table 2.2. Discovering alternative ways to inhibit and eliminate bacterial biofilm growth on medical devices is urgently needed. One of the promising strategies is applying nanotechnology in antibacterial polymer materials, as it directly contacts the bacterial cell wall and destroys bacterial compartments.

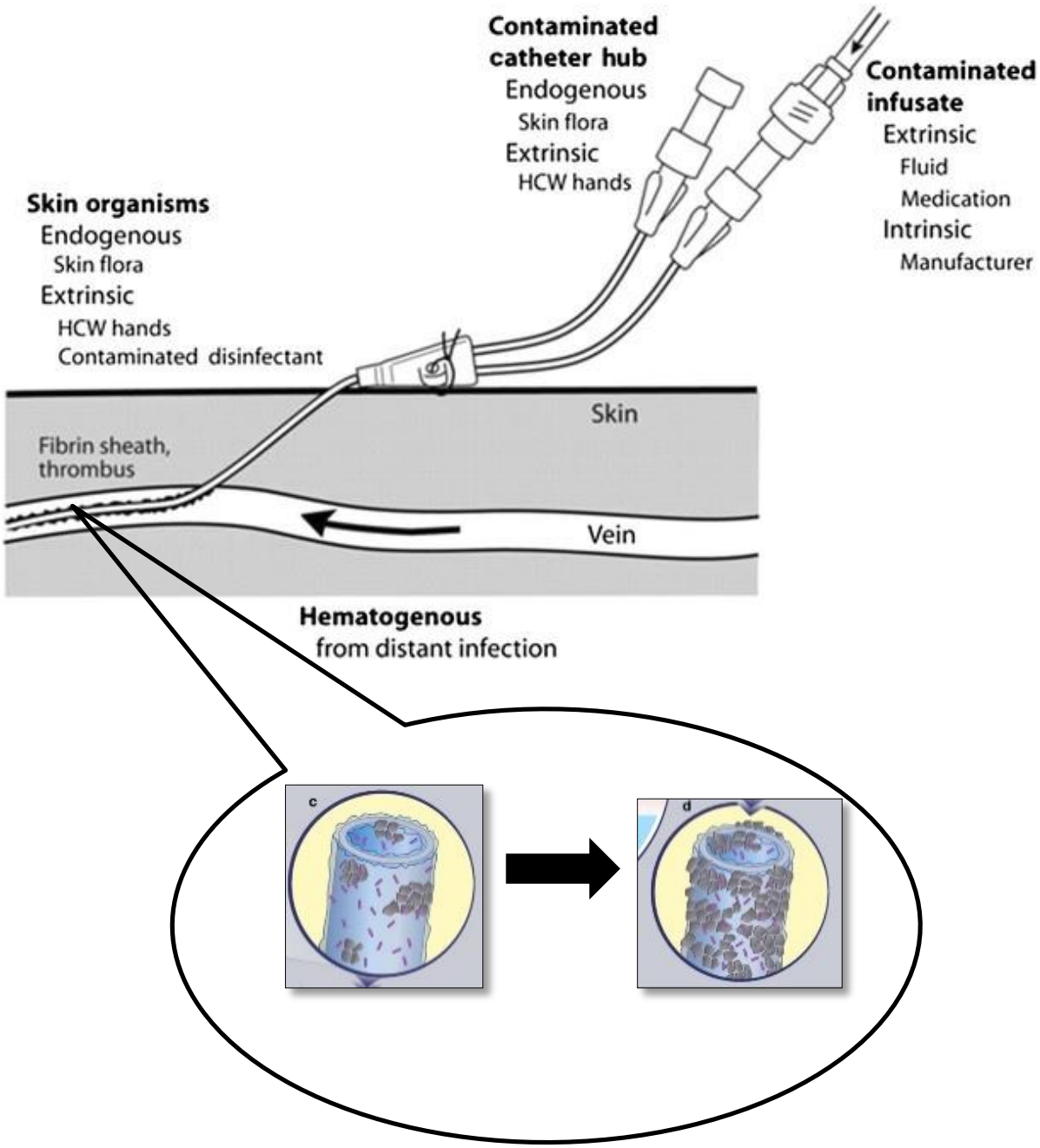

Figure 2.3 **Catheter insertion for fluid administration (medication, blood withdrawal or nutritional solutions).** Cross-contamination may create possible routes for HAI-causing organisms from the skin microflora of patients or from exogenous microflora from other sources. These organisms directly attach and develop biofilms on catheters, cause HAIs and worsen patient health (Adapted from Crnich, C.J. and Maki, D.G., 2002).

Table 2.2 List of common organisms that infect medical implants and develop biofilms.

Medical implants	Gram positive	Gram negative
Artificial voice prostheses	*Streptococcus mitis* (*S. mitis*), *Streptococcus salivarius* (*S. salivarius*), *Rothia dentocariosa* (*R. dentocariosa*), *Streptococcus sobrinus* (*S. sobrinus*), *Staphylococcus epidermidis* (*S. epidermidis*), *Stomatococcus mucilaginous* (*S. mucilaginous*)	Not recorded
Artificial hip prosthesis	*Coagulase-negative Staphylococci, β-hemolytic Streptococci, Enterococci, S. aureus, Streptococcus*	*P. mirabilis, Bacteroides species, E. coli, P. aeruginosa*
Replacement joints	*S. aureus and S. epidermidis*	Not recorded
Prosthetic heart valves	*Streptococcus viridans* (*S. viridans*), Coagulase-negative *Staphylococci, Enterococci, S. aureus*	Not recorded
Cardiac pace makers	*S. aureus*	Not recorded
CSF shunts	*S. aureus, S. epidermidis, Enterococcus*	Not recorded
Endotracheal tubes	*S. aureus, S. epidermidis*	*P. aeruginosa*
Urinary catheters	*S. epidermidis, E. faecalis*	*K. pneumoniae, P. mirabilis*
Peritoneal dialysis catheters	*Streptococci, Staphylococci*	None
Central venous catheters	*S. epidermidis, S. aureus, E. faecalis*	*K. pneumoniae, P. aeruginosa*
Contact lenses	Gram-positive cocci	*P. aeruginosa*
Dental implants	Acidogenic Gram-positive cocci *(*e.g. *Streptococcus*)	Gram-negative anaerobic oral bacteria
Implanted prosthetic devices for erectile dysfunction	*S. aureus, S. epidermidis*	Not recorded
Intrauterine contraceptive devices	*Micrococcus* sp., *Enterococcus* sp., Group B *Streptococci*	Not recorded
Orthopedic implants	Hemolytic *streptococci, Enterococci*	*P. aeruginosa, E. coli, P. mirabilis, Bacteroides* sp.
Breast implants	*S. aureus, Enterococcus, S. epidermidis*	Not recorded

2.2 Present status of synthetic biomedical polymers

The most widely used synthetic polymers to date are polyvinyl chloride, polyethylene (PE), polystyrene, polypropylene, polyurethane and polytetrafluoroethylene. Synthetic polymeric materials have gained much interest amongst researchers for medical applications from drug delivery systems, cardiovascular stents, blood bags, sutures, dialysis membrane, catheter, blood clot removal devices and orthodontic therapy (Maitz 2015; Serrano and Ameer 2012; Lendlein *et al*. 2010). The diverse applications of synthetic polymers with specialised characteristics for medical purposes are summarised in Table 2.3 (Sastri 2013; Wang *et al*. 2011; Cheng *et al*. 2006).

Table 2.3 Diverse applications of synthetic polymer in biomedical fields.

Synthetic polymer	Applications
Polyvinyl chloride (PVC)	• Catheters • Medical packaging • MRI fixtures and receiving coils
Polyethylene (PE)	• Medical packaging • Tubing • IV fluid bottles • Drug delivery systems, • Arthroscopy sutures • Acetabular joint • Sutures • Heart valves
Polystyrene (PS)	• Catheter trays • Suction canisters • Medical packaging • Medical and diagnostic devices
Polypropylene (PP)	• Medical packaging • Drapes and gowns • Sutures and syringes
Polyurethane (PU)	• Pacemaker • Catheter and catheter balloons • Feeding tubes
Polytetrafluoroethylene (PTFE)	• Catheters • Coating stem prostheses • Aneurysm clips • Endoscope sheaths
Polyethylene glycol (PEG)	• Drug carrier

Synthetic polymeric biomaterial devices are a promising alternative to biomedical devices with reduced immunological and inflammatory responses. Amongst all the listed synthetic polymers, PE is the most common thermoplastic produced globally because of its excellent mechanical properties, chemical inertness, low-cost production and ease of manufacturing process (Su *et al*. 2020; Khanam and Al Maadeed, 2015). PE is a group of monomer ethane and produced through several ways of polymerisation, such as radical, anionic and cationic polymerisation, which result in different types of PE (Malpass, 2010). Other studies proved that PE has high versatility and excellent biocompatibility. Both properties contribute to the application of PE in a wide range of implants and in cardiovascular therapy (Paxton *et al*. 2019).

PE has a density between 0.88 and 0.97 g per cm^3, different melting points and a branching structure. Different branching structures affect the crystallinity of PE, because a high branching degree of PE backbone will reduce the size of crystalline regions and crystallinity weight, which give the elastomeric and ductile mechanical properties of PE for a wide range of industrial applications (Koerner and Koerner, 2018). PE is classified into several types as shown in Table 2.4 as defined by the American Society for Testing and Materials (ASTM D1249, D883 and F412; ASTM, 2017).

Table 2.4 A comparison of four different types of polyethylene polymer. Structures and common biomedical applications of different polymer properties include differences in branch structure, biomedical applications, density, and melting points. (Adapted from McKeen, 2014).

Branching structure	Density and melting points	Properties	Biomedical applications	Ref
	HDPE Density = 0.94-0.97 g/cm3 Melting point = 128-136 ºC	• Lowest degree of branching with carbon and hydrogen elements in its polymer backbone • It has a more rigid surface and susceptible to stress cracking.	• OMNIPORE® • Craniofacial reconstruction • Balloon catheters • MEDPOR® HDPE • Orthopedic prostheses and implants.	Paxton *et al*. 2019
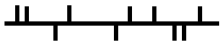	**Linear low-density PE (LLDPE)** Density = 0.90-0.93 g/cm3 Melting point = 100-130 ºC	• It is substantially linear form of LDPE and has relatively more short branches on its backbone produced by copolymerization of ethylene and higher olefins. • These short branches had increased their tensile strength, flexibility, better stress cracking adjustment and resistance against penetration and chemical.	• Dilators and sheaths • Implants	Tharayil *et al*. 2019
	Low-density PE (LDPE) Density = 0.92-0.94 g/cm3 Melting point = 105-115 ºC	• Has high degree of short and irregular long branching in its molecular chain which reduce the ability to form crystallinity contents. Thus, reduce the strength of intermolecular and interaction in London dispersion forces.	• Medical packaging • Meshes • Urinary catheters • Artificial joints	Thome *et al*. 2012; Raad *et al*. 2008; Freytag *et al*. 2003
	MDPE Density = 0.93-0.94 g/cm3 Melting point = 120-130 ºC	• It has a slightly lower density, lower hardness and rigidity and more branches than HDPE. • It has an excellent structure to resist chemical reaction, shock resistance and stable at room temperature	• Not reported	Klyosov, 2007; Vasile and Pascu, 2005

2.2.1 Implementation of metal oxide nanocomposites in biomedical polymers

Nanocomposite is a term used for nanomaterials, such as nanoparticles, nanofibres and nanoclays, which are composed of several phases in nanometre size. Metal oxide nanocomposites is composed of two or more solid materials incorporated together purposely to improve surface per volume ratio, as well as mechanical and optical properties (Omanović-Mikličanin *et al*. 2019). The incorporation of MNPs into polymer matrices is one way to increase the applications of nanoparticles and enhance their physicochemical properties. Many researchers demonstrated the application of MNP polymer nanocomposites in biomedical products, especially as antibacterial agents (Sánchez-López *et al*. 2020; Shabatina *et al*. 2020; Nikolova *et al*. 2020; Zare and Shabani, 2016).

An antibacterial polymer is consisted of two essential components: a polymer matrix and an antibacterial agent. Antibacterial polymers can be categorised into two types based on its antibacterial mechanism: passive (repelling) or active (killing) action (Huang *et al*. 2016). Passive antibacterial polymers prevent bacterial attachments on their surface through hydrophilic or hydrophobic and electrostatic repulsions and the low surface free energy of the matrix. Several polymers, such as polyethylene glycol, poly(2-methyl-2-oxazoline) and poly (sulfobetaine methacrylate), prevent bacterial adhesion through neutral polymer brush systems and the dual function of the antimicrobial surface of poly(L-lysine)-graft-poly(2-methyl-2-oxazoline) quaternary ammonium on polymer surface (Yu *et al*. 2014; Pidhatika and Rakhmatullina 2014).

In comparison, active antibacterial polymers kill bacteria through electrostatic and biocidal interactions. Active antibacterial agents, such as quaternary ammonium, are functionalised within the polymer matrix to kill bacteria by adhering to the bacterial cell wall through electrostatic interaction, entering the cytoplasmic membrane and destroying bacterial intracellular membrane to lead to cell death (Xue *et al*. 2015). Individual MNPs tend to aggregate. MNPs with low selectivity and weak mechanical strength are improved by functionalisation with polymers before implementation in real-life applications (Sarkar *et al.* 2012). Moreover, efficacy in antibacterial actions could be enhanced through polymerisation to prolong the lifetime of antibacterial materials (Kenawy *et al*. 2007).

Both elements can be synthesised *ex situ* or *in situ.* In top-down *ex situ* synthesis, MNPs are synthesised individually prior to intercalation with a polymer. MNPs are embedded into polymer via physical entrapment through casting and solvent evaporation, chemical polymerisation and co-precipitation. This process will further form polymer membrane or crosslinking between each element to develop a 3D framework after sonication to ensure that the MNPs are dispersed evenly within the polymer matrix (Guo *et al*. 2014). *In situ* synthesis is a one-step fabrication method that allows MNP synthesis within a pre-formed polymer matrix (Sarkar *et al.* 2012). The applications of MNPs as antibacterial filler in polymer matrix are summarised in Table 2.5.

Table 2.5 **Overview of MNPs applications as antibacterial agent**. MNPs are embedded with polymer nanocomposites as antibacterial agents for biomedical purposes.

Synthetic Polymers used	MNPs	Antibacterial testing	Findings	Ref
PEG	Zinc oxide		A shorter reaction time of PEG capped ZnO NPs have higher antibacterial activity. Discrete antibacterial mechanisms via the generation of ROS and hydrogen peroxide from ZnO NPs.	Meshram *et al*. (2018)
	Copper oxide	MIC and disc diffusion	CuO:PEG showed lower MIC concentration. Generation of ROS via deposition of CuO NPs on the surface of bacteria were purpose responsible for antibacterial activity.	Hemalatha and Akilandeswari, (2016).
Ecoflex	Zinc oxide	Agar diffusion tests Time-kill assay	The lesser inhibition average halo values for the E. coli (0.67 cm) compared with S. aureus (1.13 cm) due to the structure membrane's difference after being treated with ZnO NPs. Polymer ZnO NPs (1%) did show great reduction (0.5% of survived S.aureus colonies) after be treated for 24 hours.	Capelezzo *et al*. (2018)
Linear low-density PE (LLDPE)	Titanium and zinc oxide	ASTM E2149	LLDPE nanocomposites with a higher ratio of ZnO NPs did show remarkable efficacy against both pathogens. Two primary mechanisms played a significant role in the bacteriostatic effect; generation of ROS and zinc ions release.	Saharudin *et al*. (2018)
	Cuprous oxide	Broth dilution	Composite demonstrated the highest antibacterial activity against both pathogens through thermal adhesion to the polymer with zero copper leaching. The bactericidal activity was purpose due to direct contact with a polymer surface.	Gurianov *et al*. (2019)
Low-density PE (LDPE)	Lithium-Titanate/	ASTM E2149	Reduction in crystallinity and enhancement in the LDPE matrix's polarity and hygroscopic properties did improve an excellent water uptake for ROS and metal ion release. Therefore, it helps the inactivation of *S. aureus.*	Basiron *et al*. 2019
LDPE and EVA	Silver oxide and Titanium dioxide	CFU counts	A higher % of Ag-TiO_2 nanocomposites in polymer having the most reduction in *E. coli* bacterial colony. It showed the bacteriostatic ability of Ag-TiO_2 to interact with an outer complex of LPS, phospholipids and lipopolyproteins.	da Olyveira *et al.* 2011

Table 2.5 Overview of MNPs applications as antibacterial agent. MNPs are embedded with polymer nanocomposites as antibacterial agents for biomedical purposes **(**continued)

Synthetic Polymers used	MNPs	Antibacterial testing	Findings	Ref
LDPE and EVA	Silver oxide and Titanium dioxide	CFU counts	A higher % of Ag-TiO_2 nanocomposites in polymer having the most reduction in *E. coli* bacterial colony. It showed the bacteriostatic ability of Ag-TiO_2 to interact with an outer complex of LPS, phospholipids and lipopolyproteins.	da Olyveira *et al.* 2011
PP	Copper oxide	CFU counts	Direct contact of PP composites with CuO NPs fillers surfaces able to kill Gram-negative *E. coli* strains within 4 hours of treatment periods.	Delgado *et al*. 2011
	Zinc oxide	CFU counts	The release of Zn^{2+} from the PP/ZnO nanocomposites destroy the cell walls of *E. coli* due to direct contact with the surface. Besides, the generation of ROS (HO, H_2O_2, O^{2-}) under light irradiation also damages the bacterial cell membranes.	Prasert *et al*. 2020
PVC	Zinc oxide, Titanium dioxide and ferrix oxide	CFU counts	The 10 wt.% of Fe_2O_3, ZnO, and TiO_2 NPs embedded into PVC exhibit significant inhibition of Gram-positive and Gram-negative bacteria compared with 15 wt.%. It showed ZnO and Fe_2O_3 NPs had much better antibacterial activity against Gram positive bacterial strains. Whereas, TiO_2 had better antibacterial activity against Gram-negative bacteria. The size of NPs did influences the efficacy of antibacterial activity.	Sadek *et al*. 2020
PU	Silver and zinc oxide	OD and CFU counts	It revealed an excellent bactericidal and bacteriostatic activity of PUZnAg composite nanofibers against Gram positive (*S. aureus* and *B. subtilis*) and Gram negative (*E. coli*) strains. Enhancement in antibacterial activity been observed when both nanocomposites were combined within PU.	Jatoi *et al*. 2020

2.2.2 Antibacterial potential of TiO_2 and ZnO nanocomposites

Amongst the metal oxide antibacterial agents listed, TiO_2 and ZnO are the most valuable semiconducting oxide nanoparticles and considered "generally recognised as safe (GRAS)" by the American Food and Drug Administration to be used in all industries (FDA, 2016). Safety is an essential factor that needs to be considered in developing antibacterial polymer nanocomposites for human applications. The nanocomposite needs to be nontoxic and must not react with the polymer. Both semiconductors are activated and react with H_2O or hydroxide ions adsorbed on the surface upon UV light excitement to generate highly active ROS, including hydroxyl radicals (·OH), superoxide (O_2•$^-$) and hydrogen peroxide (H_2O_2) (Jaskova *et al.*, 2013). In this case, ·OH and O_2•$^-$ will attach on the cell surface and H_2O_2 will penetrate into bacterial cells to kill the bacteria as shown in Figure 2.4.

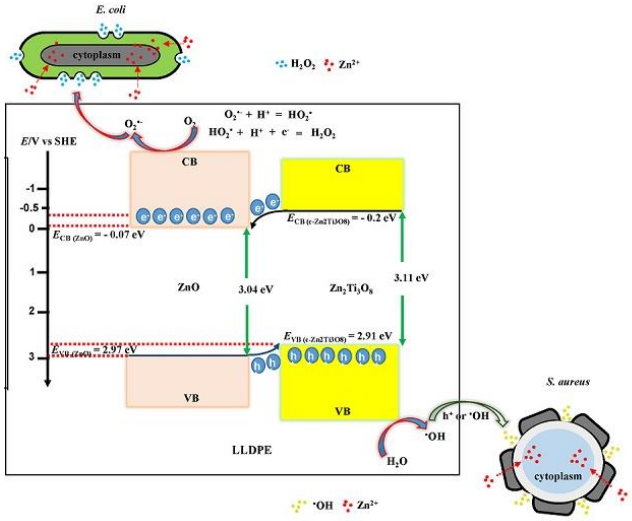

Figure 2.4 Schematic diagram of visible light induced photocatalytic of TiO_2/ZnO photonic nanocomposites. TiO_2/ZnO nanocomposites performed an excellent photocatalytic and antibacterial activities against both Gram-positive and Gram-negative pathogens (Adapted from Padmavathy and Vijayaraghavan 2008).

Toxic ions from ZnO and oxidative stress induced by ROS generation also cause cell death. TiO_2 is thermally stable, whereas ZnO has an amphoteric nature and can react with acids and alkali. The antibacterial properties of ZnO depend on high surface area per volume ratio and the release of Zn^{2+}. ZnO generates free Zn^{2+} ions when immersed in solution and immediately binds to biomolecules, such as proteins, carbohydrates, lipids and nucleic acid. The released Zn^{2+} ions spontaneously attach to the bacterial surface because of electrostatic forces and react with the bacterial respiratory enzymes' thiol group. Zn^{2+} ions increase ROS production and develop oxidative stress in cells (Siddiqi *et al*. 2018). The accumulation of Zn^{2+} ions and oxidative stress generation disrupt several targets, such as bacterial membrane, carbohydrates, nucleic acids, amino acids, protein, lipid and DNA (Du *et al*. 2004; Agarwal *et al*. 2018). Biocidal effects are caused by the disruption of metabolic pathway and protein synthesis (Sirelkhatim *et al*. 2015).

The wide band gaps at ~3.2 eV for TiO_2 and 3.37 eV for ZnO nanoparticles, the high recombination of photogenerated electron–hole pairs, low light harvesting efficiency, weak photoresponse, inefficient charge transport and separation hinder the complete bacterial inhibition caused by single metal oxide nanoparticles (Mondal 2017; Kudo and Miseki 2009). These drawbacks render both semiconductors photocatalytically inactive at higher wavelengths of the electromagnetic spectrum. Alternative strategies, such as metal or metal oxide doping, co-doping and coupling with other semiconductors, can be applied to solve these limitations and extend the photoresponse in the visible light region (Cai *et al*. 2014; Vallejo *et al*. 2020).